Laser and Particle Beams

cambridge.org/lpb

Collision-less shocks and solitons in dense laser-produced Fermi plasma

J. Goswami[1], S. Chandra[2], J. Sarkar[1], S. Chaudhuri[1] and B. Ghosh[1]

[1]Department of Physics, Jadavpur University, Kolkata 700032, India and [2]Department of Physics, Goverment General Degree College at Kushmandi, Dakshin Dinajpur 733121, India

Research Article

Cite this article: Goswami J, Chandra S, Sarkar J, Chaudhuri S, Ghosh B (2020). Collision-less shocks and solitons in dense laser-produced Fermi plasma. *Laser and Particle Beams* **38**, 25–38. https://doi.org/10.1017/S0263034619000764

Received: 6 October 2019
Revised: 26 October 2019
Accepted: 15 December 2019
First published online: 20 January 2020

Keywords:
Dense plasma; finite temperature; laser–plasma interaction; shocks; solitons

Author for correspondence: S. Chandra, Department of Physics, Goverment General Degree College at Kushmandi, Dakshin Dinajpur 733121, India. E-mail: swarniv147@gmail.com

Abstract

The theoretical investigation of shocks and solitary structures in a dense quantum plasma containing electrons at finite temperature, nondegenerate cold electrons, and stationary ions has been carried out. A linear dispersion relation is derived for the corresponding electron acoustic waves. The solitary structures of small nonlinearity have been studied by using the standard reductive perturbation method. We have considered collisions to be absent, and the shocks arise out of viscous force. Furthermore, with the help of a standard reductive perturbation technique, a KdV–Burger equation has been derived and analyzed numerically. Under limiting cases, we have also obtained the KdV solitary profiles and studied the parametric dependence. The results are important in explaining the many phenomena of the laser–plasma interaction of dense plasma showing quantum effects.

Introduction

Laser-produced plasmas and laser–plasma interactions have been of increased interest these days. Often lasers of 10^{22} W/m^2 intensity and pulse duration of few picoseconds are used in these laser–plasma experiments. The density of plasma is what is important here. The density and temperature of the plasma may exhibit thermal or quantum behavior. The thermodynamic as well as the physical parameters show significant deviations from the general nature of the plasma. The ponderomotive force plays an important role. It may produce shocks, double layers, solitary profiles, or similar stationary structures under various plasma situations. Shocks appear when different fluids corresponding to plasma species approach each other with speed greater than the local acoustic speed known as strong shock. Moreover, there is another kind of shock which can be formed when two fluids collide a subsonic speed which is known as weak shock (Zel'dovich and Raizer, 1966; Landau and Sykes, 1959). Energy dissipation and associated rapid fluctuation of pressure, temperature, and volume are observed (Jagadeesh, 2008). Such shocks are described by the laser-piston model (Henis *et al.*, 2019). According to this theory, the double layer structure (often termed as laser piston) drives a compressive shock wave which moves in the unperturbed dense plasma. The piston structure and the relation between its velocity and laser intensity were simulated by Esirkepov *et al.* (2004), Schlegel *et al.* (2009), Naumova *et al.* (2009), Eliezer *et al.* (2014), and very recently by Schmidt and Boine-Frankenheim (2016). The mechanism allows the particle to obtain very high velocities and was reported earlier by Macchi *et al.* (2013) and prior to him by Robinson *et al.* (2009). Hora (2012) has carried out two fluid simulations of laser–plasma interactions with predominantly nonlinear ponderomotive force. Based on the place of occurrence, shocks can be observed in space (Saitou *et al.*, 2012) or laboratory-produced plasmas (Bailung *et al.*, 2011). Our interest is towards plasma–laser interactions. Based on the interparticle interaction, shocks may be collisional or without collision. In the former case, the kinetic energy is supplied by Coulomb collision, a binary elastic collision between two charged particles interacting through their own electric fields. Here, the shock front is narrower and width is few mean free path of binary collision. On the other hand, if there is no collisional effects, the shocks experience instabilities due to collective phenomena (or ionic reflections from the shock front) that provide the excess energy to be dissipated at the front. Here, the thickness is even narrower and is many times smaller than the mean free path. Theobald *et al.* (2006) have reported an instance containing supra-thermal particles.

Now under extreme densities where the particle de Broglie waves come very close, quantum tunneling effects are important. We accordingly incorporate the quantum diffraction effects through the Bohm term (Haas, 2011). The electron experiences a pressure due to its quantum effects. Such pressure can be of different forms, like Fermi pressure (Haas *et al.*, 2003; Misra and Bhowmik, 2007; Chandra, 2016), relativistic pressure (Chandra and Ghosh, 2012; Chandra *et al.*, 2013; Ghosh and Chandra, 2013), or even certain other effects due to thermal anisotropy (Chandra and Ghosh, 2013), where as a result of such anisotropy violation

CAMBRIDGE UNIVERSITY PRESS

of the incompresibility of the fluid in phase space is theorized (Shukla and Eliasson, 2010; Chandra and Ghosh, 2013). Such finite temperature effect incorporated by Elliasson and Shukla has been used in some works in recent days (Akbari-Moghanjoughi, 2012; Akbari-Moghanjoughi and Eliasson, 2016). In a laser–plasma interaction, despite the density being very high and can exhibit Bohm potential effects, the finite temperature may cause deviation from extreme quantum plasma situation and the systems need to be formulated accordingly. Certain authors (Lakhina, 1995; Devanandhan *et al.*, 2011; Chandra *et al.*, 2012; Goswami *et al.*, 2019) have studied shocks in many dense astrophysical plasma. But, within our experimental ambit with dense plasma interacting with intense laser beam, a proper physical phenomena need to be investigated. Our work is motivated by the idea of studying certain thermal anisotropy due to laser beam (or pulse) in a dense quantum plasma. The results of our study will identify many parametric domains that can sustain solitary structure or shocks and the conversion between them.

The paper is organized in the following pattern. In the "Basic equation" section, we set our governing equations and with proper normalization we have simplified them. In the next two sections, we obtain the linear dispersion relations and analyze the results from them. In "Derivation of the KdV–Burger's equation and Shocks and solitary formation" sections, we derive the structure for shocks and solitons and finally discuss the result with associated figures. Lastly, we conclude with the probable applications of our findings and scope for future work.

Basic equation

We consider nonlinear propagation of electron acoustic waves in an unmagnetized two component quantum plasma experiencing viscous effects consisting electrons at finite temperature and Boltzmann distributed ions.

Based on the three-dimensional equilibrium Fermi–Dirac distribution for electrons at an arbitrary temperature, Shukla and Eliasson (2010) derived a set of fluid equation which are valid at both extremely low temperature and finite temperature limits. A plane longitudinal electrostatic wave propagates in quantum plasma without collision and leads to adiabatic compression, thereby causing temperature anisotropy in the electron distribution. Due to quantum mechanical tunneling, the classical compressibility of the electron phase fluid is violated. Furthermore, the nonequilibrium dynamics of the plasma particles are considered with the assumption that the chemical potential (μ) remains constant. Under such assumptions, the nonequilibrium particle density is given by the following equation:

$$n_0 = \frac{1}{2\pi^2}\left(\frac{2m}{\hbar}\right)^{3/2}\int_0^\infty \frac{E^{1/2}\,dE}{e^{\beta(E-\mu)}+1} = -\frac{1}{2\pi^2\beta^{3/2}}\left(\frac{2m}{\hbar}\right)^{3/2}\Gamma\left(\frac{3}{2}\right)\mathrm{Li}_{3/2}(-e^{\beta\mu}) \tag{1}$$

where m is the electron mass, $\hbar$ is the reduced Plank's constant, n_0 is the equilibrium number density, $\beta = 1/k_B T_{e0}$, T_{e0} is the background temperature of electron, μ is the chemical potential, and $\mathrm{Li}_\nu(x)$ is the polylogarithmic function in x of order ν. When $\beta \to \infty$, that is, cold temperature of electron, we have $\mu \to E_F$, where E_F is the Fermi energy. Accordingly, the Fermi energy is given by the following equation:

$$E_F = (3\pi^2 n_0)^{2/3}\frac{\hbar^2}{2m} \tag{2}$$

Now, using the zeroth and first moments of the higher equations with Fermi–Dirac distribution function and assuming that the Bohm potential is independent of thermal fluctuations in such finite temperature situation, we derive the continuity and momentum equations in the following form:

$$\frac{\partial n_e}{\partial t} + \frac{\partial n_e u_e}{\partial x} = 0 \tag{3}$$

$$\left(\frac{\partial}{\partial t} + u_e\frac{\partial}{\partial x}\right)u_e = \frac{e}{m_e}\frac{\partial \varphi}{\partial x} - \frac{n_0 v_{T_e}^2}{n_e}F\frac{\partial\left(\frac{n_e}{n_0}\right)^3}{\partial x} + \frac{\hbar^2}{2m_e^2}\frac{\partial}{\partial x}\left[\frac{1}{\sqrt{n_e}}\frac{\partial^2\sqrt{n_e}}{\partial x^2}\right] + \eta\frac{\partial^2 u_e}{\partial x^2} \tag{4}$$

where n_e and u_e are the electron density and electron fluid velocity, respectively; φ is the electrostatic potential and $v_{T_e} = \sqrt{k_B T_{T_e}/m_e}$ is the thermal speed, F is the ratio of two polylogarithmic functions given by Akbari-Moghanjoughi and Eliasson (2016),

$$F = \frac{\mathrm{Li}_{5/2}(-e^{\beta\mu})}{\mathrm{Li}_{3/2}(-e^{\beta\mu})} \tag{5}$$

and corresponds to the finite temperature anisotropic distribution. The second last term in the momentum [Eq. (4)] corresponds to the Bohm potential. η is the viscosity coefficient.

The system is closed by the Poisson's equation,

$$\frac{\partial^2\varphi}{\partial x^2} = 4\pi e(n_e - n_i) \tag{6}$$

Here, we made use of the standard normalization condition which are $\bar{x} \to x/\lambda_{De}$, $\bar{t} \to \omega_{pe}t$, $\bar{\varphi} \to e\varphi/T_e$, $\bar{u_e} \to u_e/v_{T_e}$, $\bar{\eta} \to \eta/\lambda_{De}v_{T_e}$ and obtained the equations in the dimensionless form given by,

$$\frac{\partial \bar{n}_e}{\partial \bar{t}} + \frac{\partial \bar{n}_e\bar{u}_e}{\partial \bar{x}} = 0 \tag{7}$$

$$\left(\frac{\partial}{\partial \bar{t}} + \bar{u}_e\frac{\partial}{\partial \bar{x}}\right)\bar{u}_e = \frac{\partial \bar{\varphi}}{\partial \bar{x}} - \frac{3F}{\chi}\bar{n}_e\frac{\partial \bar{n}_e}{\partial \bar{x}} + \frac{H^2}{2}\frac{\partial}{\partial \bar{x}}\left[\frac{1}{\sqrt{\bar{n}_e}}\frac{\partial^2\sqrt{\bar{n}_e}}{\partial x^2}\right] + \bar{\eta}\frac{\partial^2\bar{u}_e}{\partial \bar{x}^2} \tag{8}$$

$$\frac{\partial^2\bar{\varphi}}{\partial \bar{x}^2} = \bar{n}_e - \bar{n}_i \tag{9}$$

where $\chi = (V_{F_e}/V_{T_e})^2$ and $H = \hbar\,\omega_{pe}/2k_B T_{F_e}$.

The ions follow the Boltzmann distribution as $n_i = n_{i0}\,e^{-\sigma\varphi}$. Here, $\sigma = T_i/T_e$. As the equation is normalized by the frame of the electron, we can write this simple distribution of ions considering the fact that the electrons and the ions have the different temperatures (El-Taibany *et al.*, 2019).

https://doi.org/10.1017/S0263034619000764 Published online by Cambridge University Press

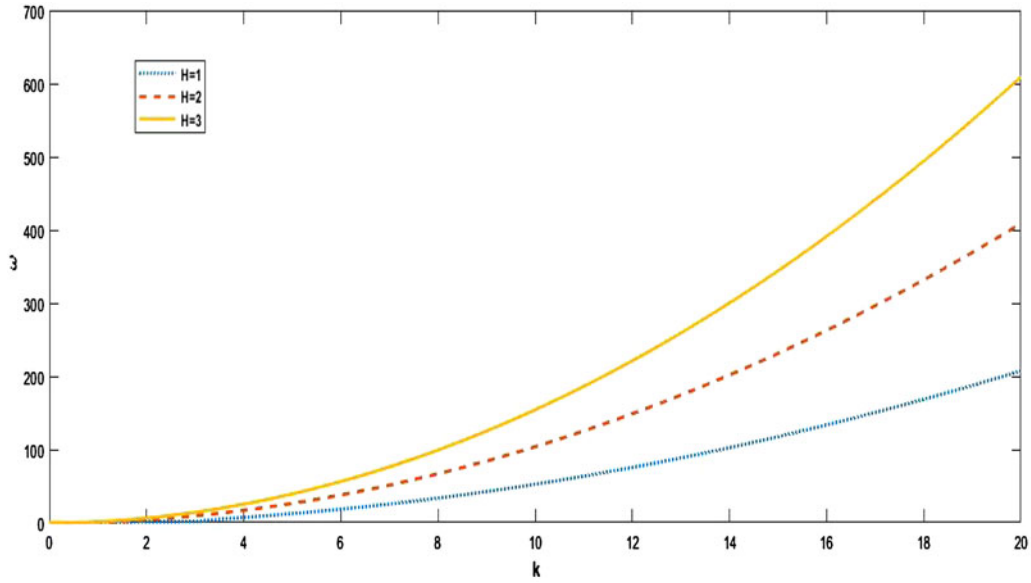

Fig. 1. Real dispersion relation for different quantum diffraction parameter (H) with $u_0 = 0.5$, $\sigma = 0.5$, $F = 1.5$, and $\chi = 0.5$.

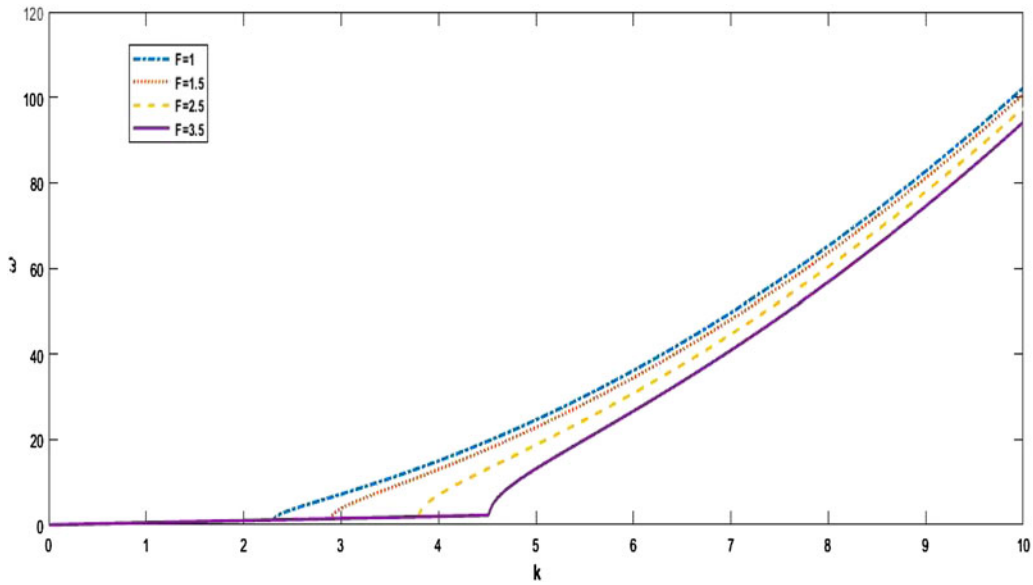

Fig. 2. Real dispersion relation for different finite temperature electron degeneracy parameter (F) with $u_0 = 0.5$, $\sigma = 0.5$, $H = 2$, and $\chi = 0.5$.

Derivation of linear dispersion relation

In order to investigate the linear and nonlinear behavior of electron acoustic wave in this two-component electron–ion plasma, we make the following perturbation expansion for the field quantities n_e, u_e, and φ about their equilibrium values:

$$\begin{bmatrix} n_e \\ u_e \\ \varphi \end{bmatrix} = \begin{bmatrix} 1 \\ u_{(0)} \\ \varphi_0 \end{bmatrix} + \varepsilon \begin{bmatrix} n_e^{(1)} \\ u_e^{(1)} \\ \varphi^{(1)} \end{bmatrix} + \varepsilon^2 \begin{bmatrix} n_e^{(2)} \\ u_e^{(2)} \\ \varphi^{(2)} \end{bmatrix} + \cdots \tag{10}$$

We assumed that all field variables varying as $\exp[i(kx - \omega t)]$ and accordingly for normalized wave frequency (ω) and wave number (k) [which contains both real and imaginary part], the linear dispersion relation. Here, the viscous term plays a very pivotal role. The dispersion equation has an exponentially decaying complex part in addition to the real dispersion relation. In this case if we substitute the wave number with a real plus imaginary parts (given by $k = k_r + ik_i$), we obtain the two dispersion relations given by,

$$\omega' = k_r u_0 \pm \sqrt{k_r^2 u_0^2 - \frac{(\sigma - \sigma^2\varphi_0 + k_r^2)\left(\frac{3F}{\chi}k_r^2 + \frac{H^2 k_r^4}{4} - k_r^2 u_0^2\right) + k_r^2}{\sigma - \sigma^2\varphi_0 + k_r^2}} \tag{11}$$

https://doi.org/10.1017/S0263034619000764 Published online by Cambridge University Press

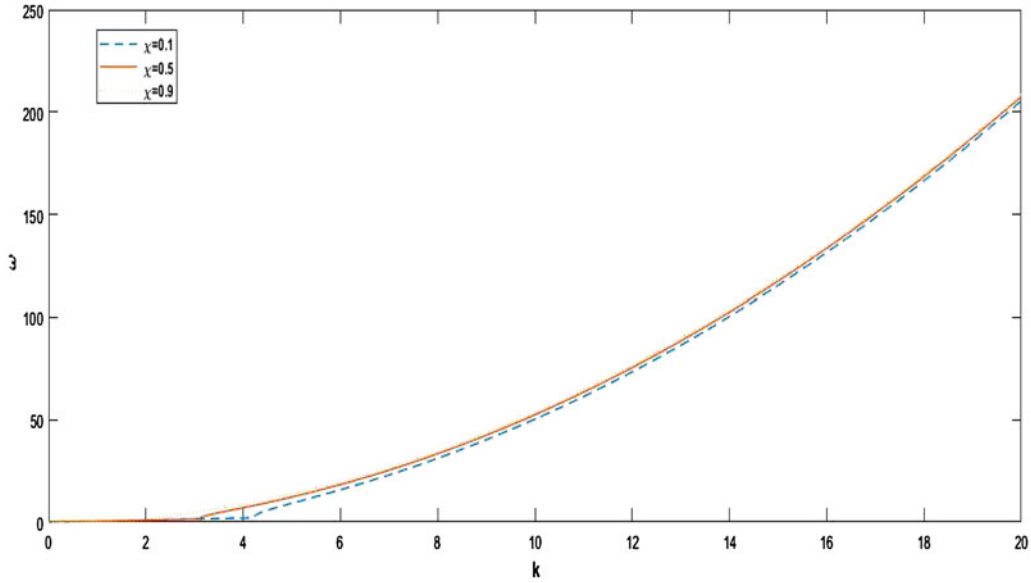

Fig. 3. Real dispersion relation for different Fermi velocity and thermal velocity ration squared (χ) with $u_0 = 0.5$, $\sigma = 0.5$, $F = 1.5$, and $H = 2$.

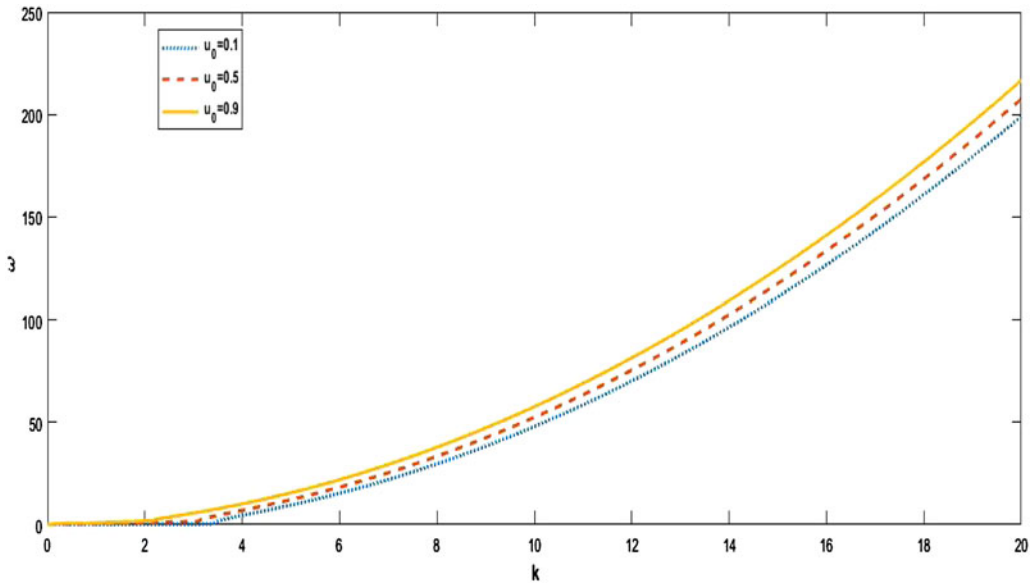

Fig. 4. Real dispersion relation for different streaming velocity (u_0) with $H = 2$, $\sigma = 0.5$, $F = 1.5$, and $\chi = 0.5$.

and

$$\omega'' = \frac{-k_i^2\eta \pm \sqrt{k_i^4\eta + \frac{12Fk_i}{\chi} + H^2k_i^3 - \frac{4k_i^3}{(\sigma\varphi_0-\sigma)(1-k_i^4)}}}{2} \quad (12)$$

Result and discussions of linear dispersion relation

The parametric variations of linear dispersion expressions for this problem have been carried out numerically. Keeping all the parameters in the range that correspond to laser–plasma interactions at such temperature and density conditions, the plots have been carried out with the quantum diffraction parameter (H) in the classical and quantum ranges and the finite temperature electron degeneracy parameter (F) corresponding to different temperature ranges. The electron to ion temperature ratio (σ), the ratio of electron Fermi velocity to electron thermal velocity (χ), the viscosity constant (η), and the streaming velocity (u_0) are among the other parameters whose variations have been studied here.

The dispersion relation consists of real and imaginary segments. The real dispersion relation corresponds to standard electron acoustic waves. When we consider the complex part of viscosity (i.e., η), it corresponds to dynamic viscosity. The real part of η therefore is no interest as we consider the wave in motion. With reference to Eq. (11), we have plotted the real dispersion relations in Figures 1–4. Here, we find that other parameters remaining constant the real dispersion curve becomes more

https://doi.org/10.1017/S0263034619000764 Published online by Cambridge University Press

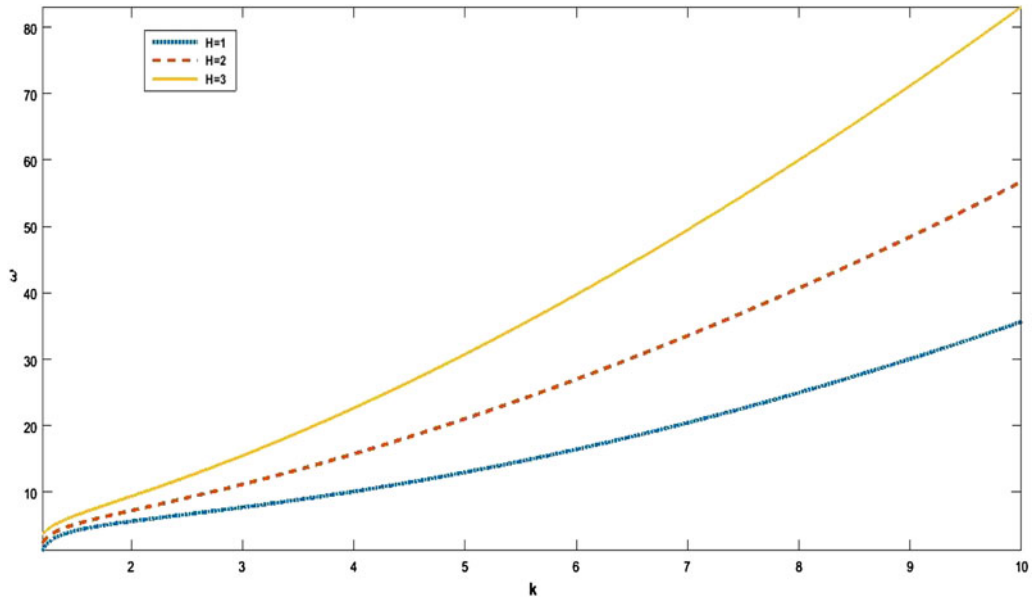

Fig. 5. Imaginary dispersion relation for different quantum diffraction parameter (H) with $\sigma = 0.5$, $F = 1.5$, and $\chi = 0.5$.

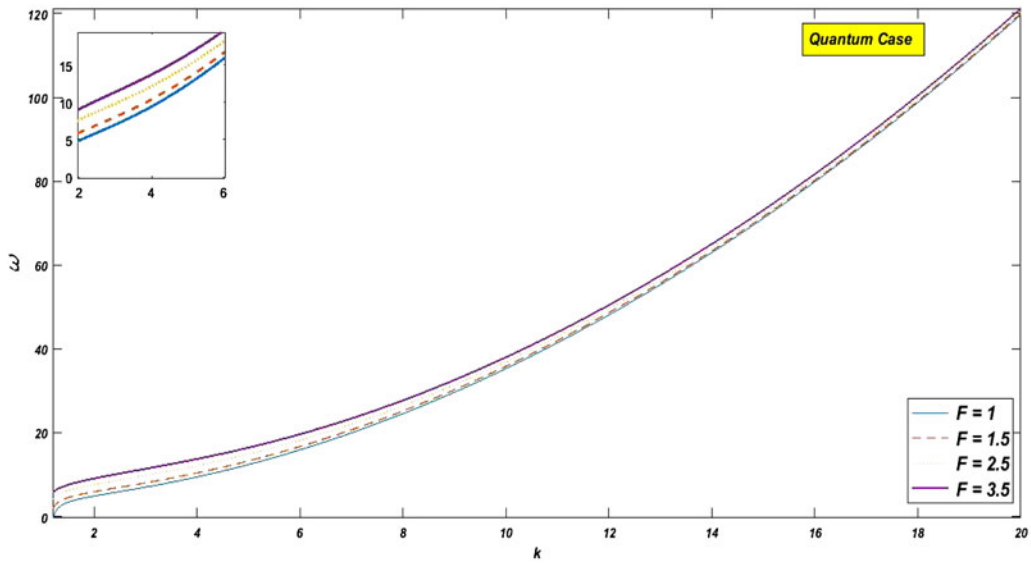

Fig. 6. Imaginary dispersion relation for different finite temperature electron degeneracy parameter (F) with $\sigma = 0.5$, $H = 2$, and $\chi = 0.5$.

steep and shows an upward trend (Fig. 1); the effect of degeneracy parameter (F) is somehow difficult. Here, there is a cutoff value for wave number to show dispersive effects. But, in the short wavelength limit, the dispersion curve shows almost negligible dependence on F (Fig. 2).

The dependence of Fermi velocity and thermal velocity ration squared (χ) shows opposite effect to F. Here as χ increases, the cutoff value of wave number recedes towards origin (Fig. 3). The streaming motion (u_0) shows (Fig. 4) both effects. An increase in the streaming speed lowers the cutoff in wave number but increases the slope. The results are in accordance with the understanding of the basic physics of plasma or fluids.

The correspondence of the effects of F and χ is related by the thermal motion. However, the effect of σ is not significant and it can be concluded that at such plasma regimes, electron and ion temperature, as well as the wave phase velocity, become insignificant. If we now consider dynamic viscosity (which is incorporated by the η term), we get a dispersion curve which corresponds to the collision-less damping, thus violating energy conservation principal characterized by Vlasov/Landau damping. In Figures 5–8, we plot the parametric dependence of the dispersion curves corresponding to such wave modes. There is a minimum value of frequency which corresponds to zero wave number and such a case has very common origin in plasma physics. The quantum diffraction shows very prominent effects in a higher wave number region (Fig. 5). In Figure 6, we find low k variations which ultimately merge into one as k-value is increased. These are similar to Figures 1 and 2.

https://doi.org/10.1017/S0263034619000764 Published online by Cambridge University Press

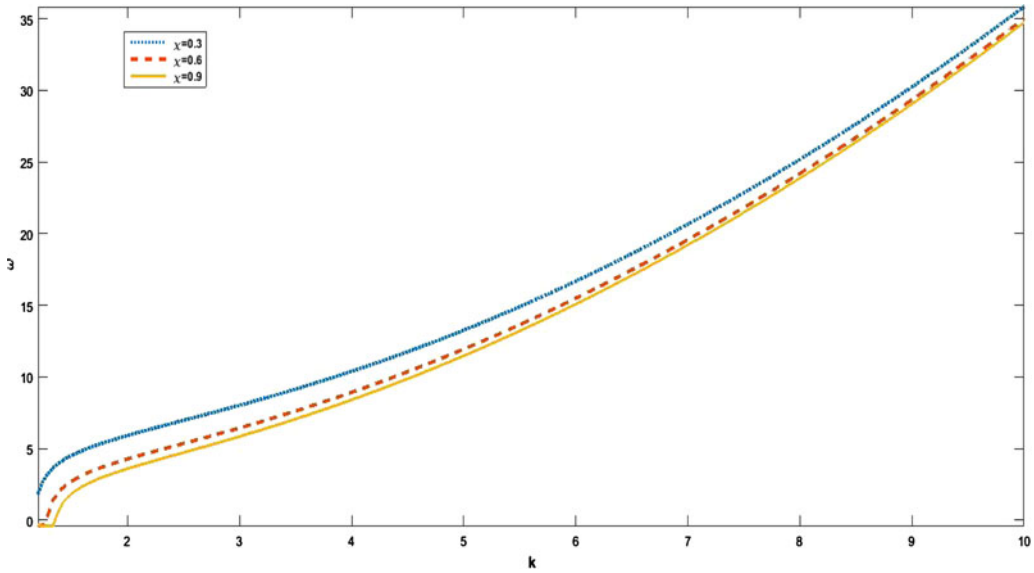

Fig. 7. Imaginary dispersion relation for different Fermi velocity and thermal velocity ration squared (χ) with $\sigma = 0.5$, $F = 1.5$, and $H = 2$.

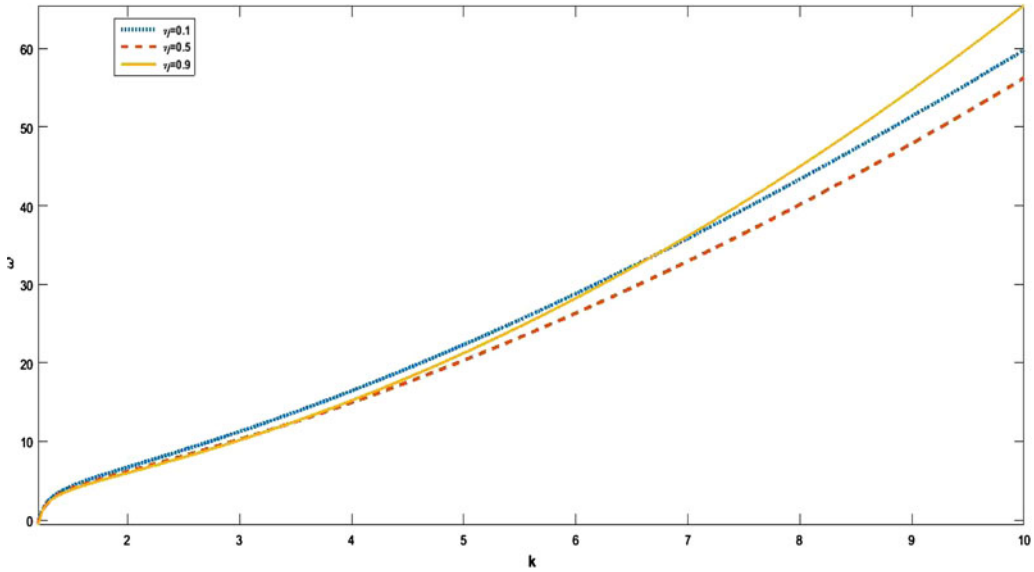

Fig. 8. Imaginary dispersion relation for different viscosity coefficient (η) with $H = 2$, $\sigma = 0.5$, $F = 1.5$, and $\chi = 0.5$.

In Figure 7, we find that χ has both effects of controlling the zero wave number frequency as well as the slope of dispersion curve. This is due to the interplay of density and thermal agitation. Figure 8 shows a rather anomalous behavior when viscosity parameter (η) is the tuning element. The results can be explained due to the dynamic nature of viscosity which indirectly depends on density, streaming motion, temperature, etc. All these are compiled and a new plot (Fig. 9) depicts the quantum and classical cases corresponding to the presence ($\eta \neq 0$) and absence ($\eta = 0$) of viscosity in the system.

Derivation of the KdV–Burger's equation

In order to derive the equation of motion for the nonlinear electron acoustic wave, we employ the reductive perturbation technique and define the following stretched variables,

$$\psi = \varepsilon^{1/2}(x - Mt) \tag{13}$$

$$\tau = \varepsilon^{3/2}t \tag{14}$$

$$\eta = \varepsilon^{1/2}\eta_0 \tag{15}$$

where ε is a small parameter which characterizes the strength of nonlinearity, and M is the phase velocity of the wave. The stretching in η is due to the small variations in perpendicular directions.

Now, Eqs (7–9) are written in terms of the stretched coordinates ψ, τ, and η and substituting of perturbation expansion

https://doi.org/10.1017/S0263034619000764 Published online by Cambridge University Press

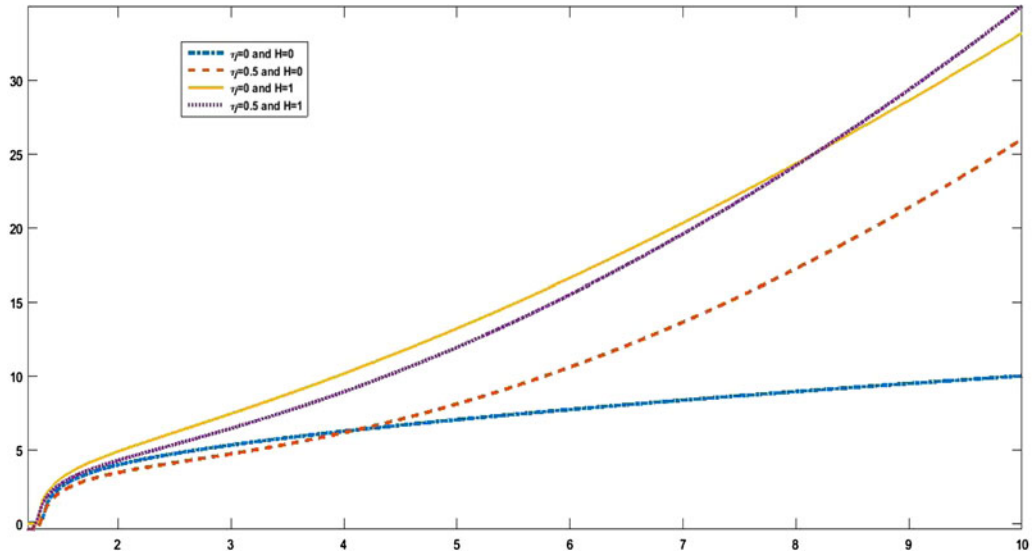

Fig. 9. Imaginary dispersion relation for quantum and classical cases.

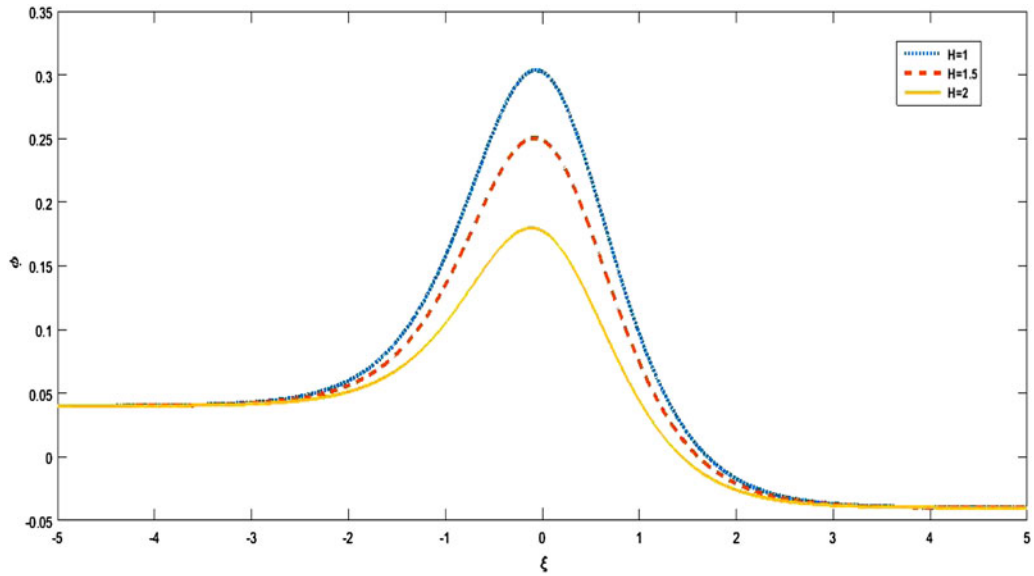

Fig. 10. Shock fronts for different quantum diffraction parameter (H) with $M = 0.7$, $u_0 = 0.5$, $\sigma = 0.5$, $F = 1.5$, $\eta_0 = 0.5$, and $\chi = 0.5$.

given in Eq. (10). From these equations, lowest orders in ε (i.e., ε) with the boundary conditions that all variables, that is, $n_e^{(1)}$, $u_e^{(1)}$, and $\varphi^{(1)}$, tend to zero as $\psi \to \pm\infty$, the first-order terms are

$$u_e^{(1)} = (M - u_0) n_e^{(1)}$$

and

$$u_e^{(1)} = \frac{\chi (M - u_0)}{3F - \chi (M - u_0)^2} \varphi^{(1)} \tag{16}$$

or

$$n_e^{(1)} = \frac{\chi}{3F - \chi (M - u_0)^2} \varphi^{(1)} \tag{17}$$

Going to next higher order terms in ε, that is, $\varepsilon^{5/2}$th term, we get

$$\begin{aligned} (M - u_0) \frac{\partial n_e^{(2)}}{\partial \psi} = {} & \frac{\partial n_e^{(1)}}{\partial \tau} + \frac{\partial (n_e^{(1)} u_e^{(1)})}{\partial \psi} + \frac{1}{(M - u_0)} \frac{\partial u_e^{(1)}}{\partial \tau} \\ & + \frac{1}{2(M - u_0)} \frac{\partial u_e^{(1)^2}}{\partial \psi} - \frac{1}{(M - u_0)} \frac{\partial \varphi^{(2)}}{\partial \psi} \\ & + \frac{3F}{2(M - u_0)\psi} \frac{\partial n_e^{(1)^{(2)}}}{\partial \psi} + \frac{3F}{(M - u_0)\psi} \frac{\partial n_e^{(2)}}{\partial \psi} \\ & - \frac{H^2}{4(M - u_0)} \frac{\partial^3 n_e^{(1)}}{\partial \psi^3} - \frac{\eta_0}{(M - u_0)} \frac{\partial^2 u_e^{(1)}}{\partial \psi^2} \end{aligned} \tag{18}$$

https://doi.org/10.1017/S0263034619000764 Published online by Cambridge University Press

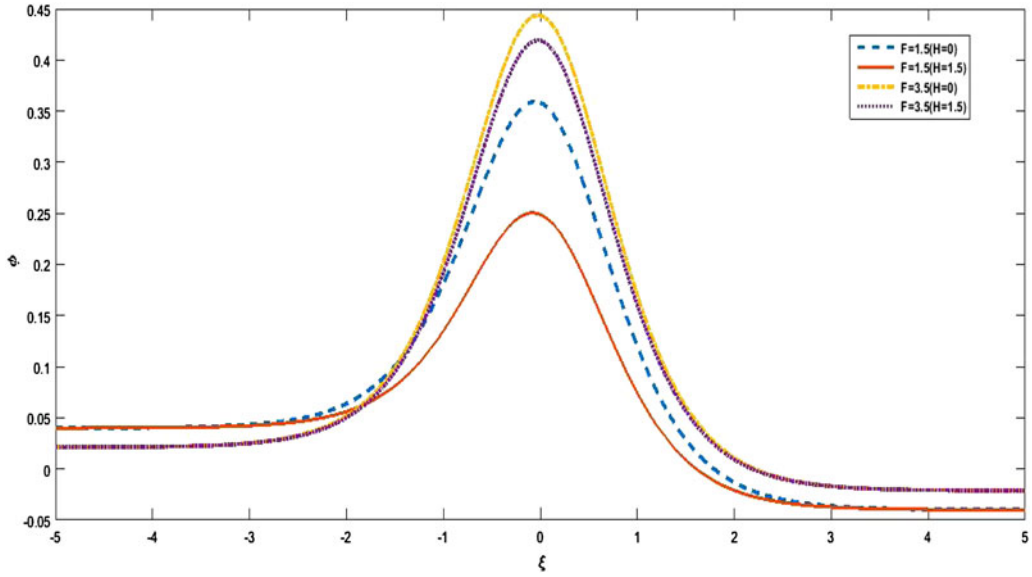

Fig. 11. Shock fronts for different finite temperature electron degeneracy parameter (F) with $M = 0.7$, $u_0 = 0.5$, $\sigma = 0.5$, $H = 1.5$, $\eta_0 = 0.5$, and $\chi = 0.5$.

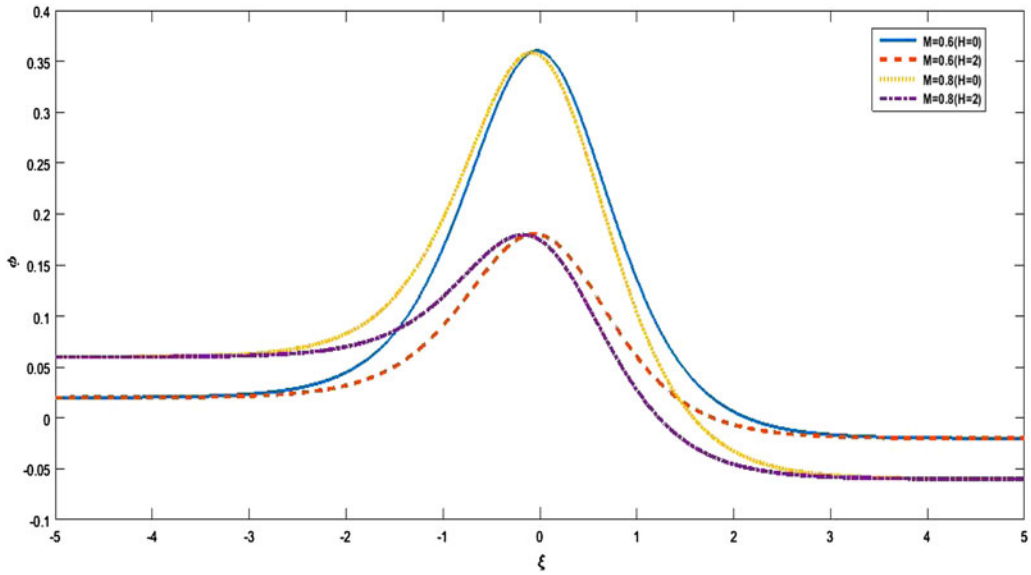

Fig. 12. Shock front for different Mach number (M) with $F = 1.5$, $u_0 = 0.5$, $\sigma = 0.5$, $H = 2$, $\eta_0 = 0.5$, and $\chi = 0.5$.

and

$$\frac{\partial u_e(2)}{\partial \psi} = \frac{1}{(M-u_0)}\frac{\partial u_e^{(1)}}{\partial \tau} + \frac{1}{2(M-u_0)}\frac{\partial u_e^{(1)^2}}{\partial \psi} - \frac{1}{M-u_0}\frac{\partial \varphi^{(2)}}{\partial \psi} + \frac{3F}{2(M-u_0)\psi}\frac{\partial n_e^{(1)^2}}{\partial \psi} + \frac{3F}{(M-u_0)\psi}\frac{\partial n_e^{(2)}}{\partial \psi} - \frac{H^2}{4(M-u_0)}\frac{\partial^3 n_e^{(1)}}{\partial \psi^3} - \frac{\eta_0}{(M-u_0)}\frac{\partial^2 u_e^{(1)}}{\partial \psi^2} \tag{19}$$

The second-order perturbation of the Poisson's equation can be equated as

$$\frac{\partial^2 \varphi^{(1)}}{\partial \psi^2} = n_e^{(2)} - n_i^{(2)} = n_e^{(2)} - \frac{\sigma^2}{2}\varphi^{(1)^2} + \sigma(1-\sigma\varphi_0)\varphi^{(2)} \tag{20}$$

Differentiating both sides of Eq. (20) by ψ and carrying out a detailed algebraic treatment with Eqs (18) and (19), the nonlinear KdV–Burger's equation is given by the following equation:

$$\frac{\partial \varphi}{\partial \tau} + A\varphi\frac{\partial \varphi}{\partial \psi} + B\frac{\partial^3 \varphi}{\partial \psi^3} - C\frac{\partial^2 \varphi}{\partial \psi^2} = 0 \tag{21}$$

https://doi.org/10.1017/S0263034619000764 Published online by Cambridge University Press

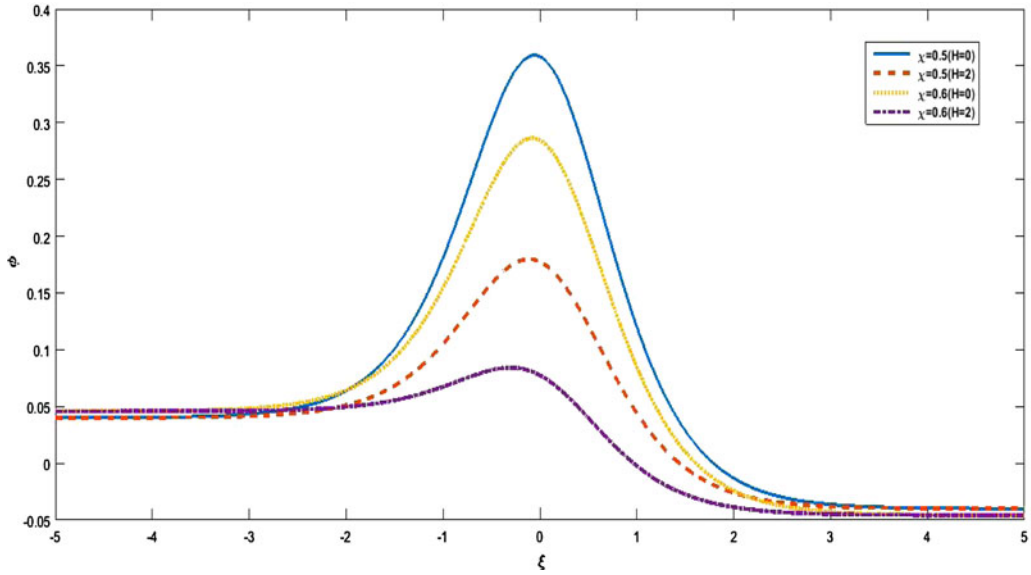

Fig. 13. Shock fronts for different ratio of electron Fermi velocity to electron thermal velocity (χ) with $F = 1.5$, $u_0 = 0.5$, $\sigma = 0.5$, $H = 2$, $\eta_0 = 0.5$, and $M = 0.7$.

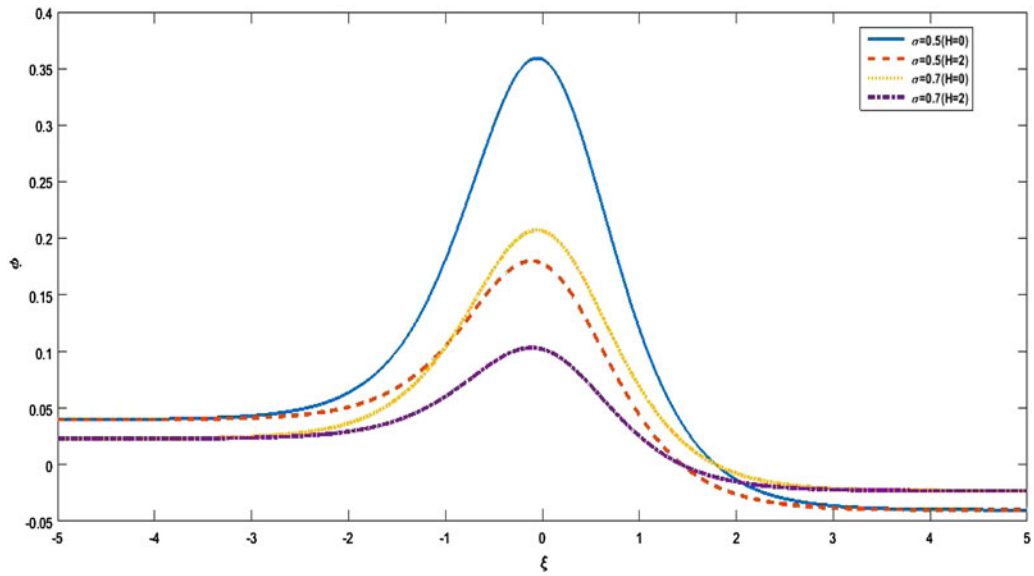

Fig. 14. Shock fronts for different electron to ion temperature ratio (σ) with $F = 1.5$, $u_0 = 0.5$, $\chi = 0.5$, $H = 2$, $\eta_0 = 0.5$, and $M = 0.7$.

Here, $\varphi = \varphi^{(1)}$, where,

$$A = \left[\frac{3(\chi(M-u_0)+3F)}{2(M-u_0)(3F-\chi(M-u_0)^2)} + \frac{\sigma^2(3F-\chi(M-u_0))^2}{2(M-u_0)\chi}\right] \tag{22}$$

$$B = \frac{4(3F-\chi(M-u_0))^2 - H^2\chi^2}{2(M-u_0)\chi^2} \tag{23}$$

$$C = -\frac{\eta_0}{2}(3F-\chi(M-u_0)^2) \tag{24}$$

It is clearly seen that if viscous coefficient $\eta_0 = 0$, then Eq. (21) reduces to KdV equation with $C = 0$. The dissipation is taken into account due to the viscous coefficient C.

The nonlinear equation obtained from Eq. (21) is the celebrated KdV–Burger's equation representing the spatio-temporal evolution of solitary structure and its transformation into shocks under limiting situation. Obtaining the solution of KdV–B, we use the standard method of hyperbolic tangent method which is often used. Using the transformation equation, $\xi = \psi - V\tau$ and the boundary condition as $\xi \to 0$ then $\varphi^{(1)} \to 0$ and $\partial\varphi^{(1)}/\partial\xi \to 0$, the KdV–B equation can be written as

$$-V\frac{d\varphi^{(1)}}{d\xi} + A\varphi^{(1)}\frac{d\varphi^{(1)}}{d\xi} + B\frac{d^2\varphi^{(1)}}{d\xi^2} + C\frac{d^3\varphi^{(1)}}{d\xi^3} = 0. \tag{25}$$

Now using the transformation $s = \tan h\xi$ and assuming a series

https://doi.org/10.1017/S0263034619000764 Published online by Cambridge University Press

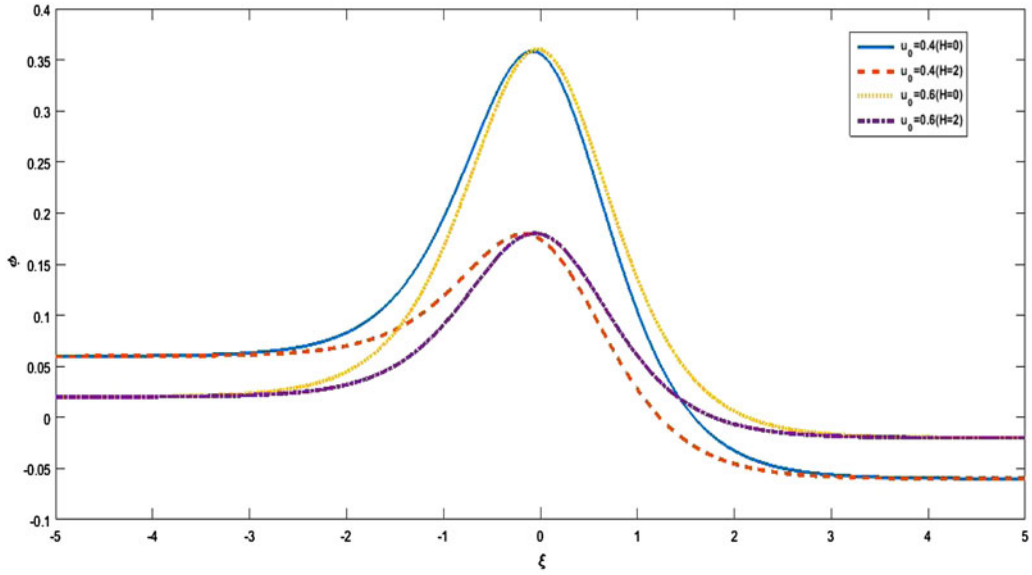

Fig. 15. Shock fronts for different streaming velocity (u_0) with $F = 1.5$, $\sigma = 0.5$, $\chi = 0.5$, $H = 2$, $\eta_0 = 0.5$, and $M = 0.7$.

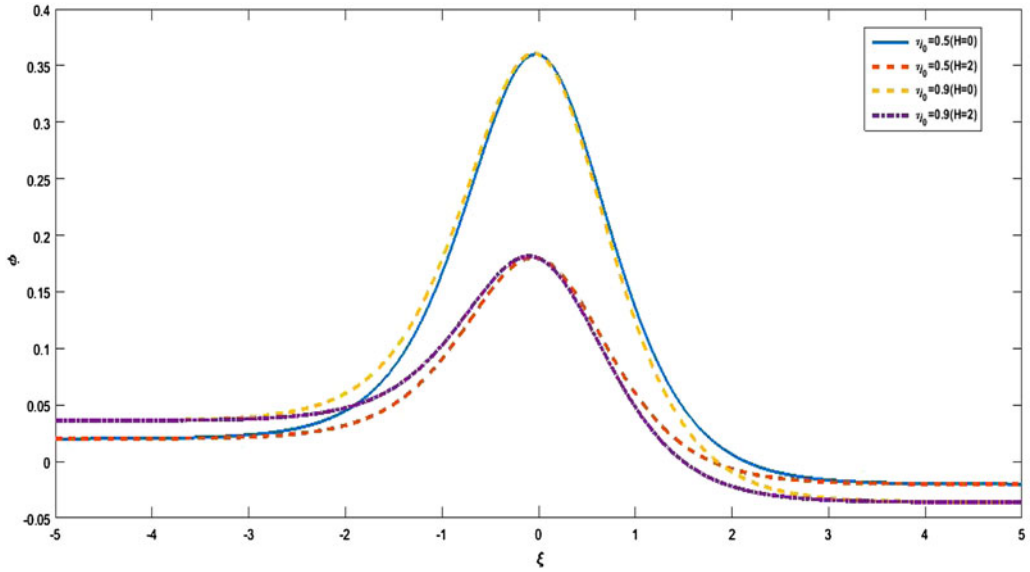

Fig. 16. Shock fronts for different viscous coefficient (η_0) with $F = 1.5$, $\sigma = 0.5$, $\chi = 0.5$, $H = 2$, $u_0 = 0.5$, and $M = 0.7$.

solution given by Wazwaz (2008) as $\varphi^{(1)}(s) = \sum_{j=0}^{n} a_j s^j$, we arrive to the solution given by

$$\varphi_1 = \frac{12B}{A}[1 - \tanh^2(\xi)] - \frac{36C}{15A}\tanh(\xi) \tag{26}$$

Here $\varphi_1 = \varphi^{(1)}$. As in Eq. (21) when $C = 0$, the equation becomes the KdV equation. Using the same transformation, we get the solution of the reduced KdV–B (standard KdV) equation given by

$$\varphi = \varphi_0 \mathrm{sech}^2 \frac{\xi}{\Delta} \tag{27}$$

where $\varphi_0 = 3V/A$ and $\Delta = 2\sqrt{V/C}$.

In the next section, we study the parametric dependence of the electrostatic shock waves and solitary formation and discuss the results with special reference to space and astronomical plasma phenomena.

Shocks and solitary formation

In the previous section, we came out with nonlinear analysis, which provided expressions for shock wave formation as well as solitary structures. Here, we have studied the parametric dependence and provide figures corresponding quantum and classical regimes. Firstly, in Figure 10, we show the variation in the quantum diffraction parameter H on shocks the higher the value of H, smaller will be the potential gaps. The dependence of shock fronts

https://doi.org/10.1017/S0263034619000764 Published online by Cambridge University Press

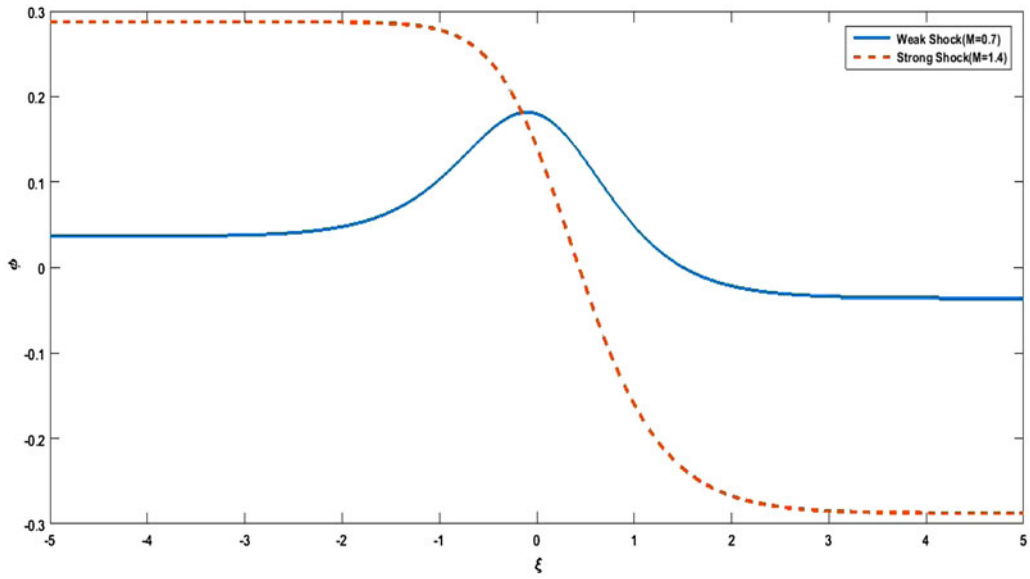

Fig. 17. Weak and strong shock front in the quantum regime ($H = 2$).

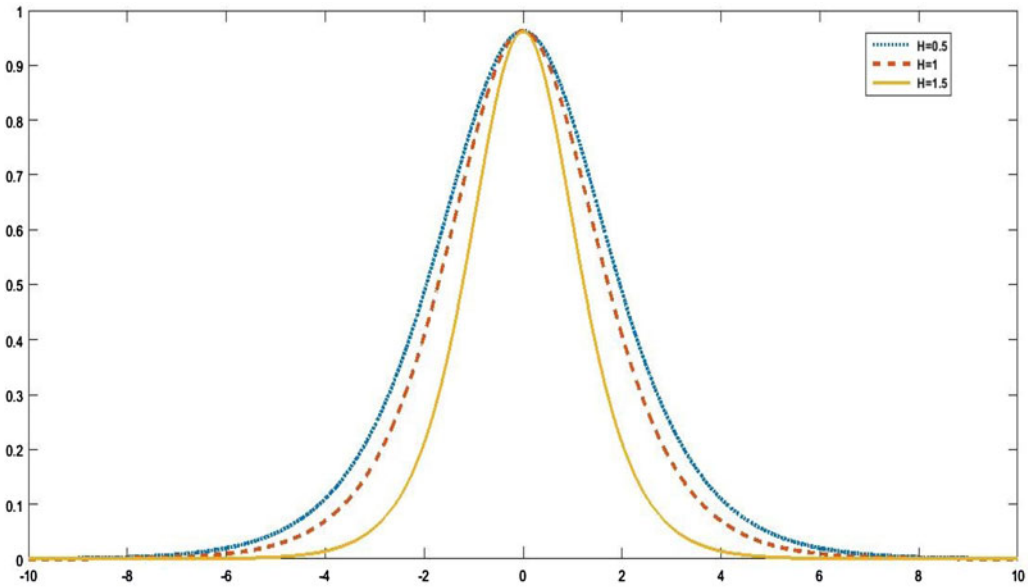

Fig. 18. Solitary structures for different quantum diffraction parameter (H) with $M = 0.7$, $u_0 = 0.5$, $\sigma = 0.5$, $F = 1.5$, and $\chi = 0.5$.

on F in the classical and quantum regime is shown in Figure 11. Figures 12–14 show corresponding parametric dependence of wave phase velocity (M), electron to ion temperature ratio (σ), and electron Fermi speed to thermal speed ration squared (χ).

In Figure 12, the phase speed shows contrasting effects on either side of the shock front and are difficult in the quantum and classical domain. Analogous effect is shown by σ (Fig. 13) but hence the potential profile difficult in height and width. However, the classical and quantum cases do not show much change. In Figure 14, the shock front at either side do not show much variation with χ, but the amplitude of the shock profile at $\psi = 0$ decreases with increase in the value of χ. Quantum and classical regimes show similar shape and formations. In Figure 15, we study the dependence on streaming velocity (u_0), which has a positive effect before the shock formation and a negative effect afterwards. The dependence of the viscosity parameter (η) is shown in Figure 16. In the quantum range, η shows a positive effect before shock formation and a negative effect after that. In the classical range, the effect is almost similar. In Figure 17, we study the weak and strong shock front by changing the wave phase velocity. In Eq. (12) we have already studied the variation of shock front for different wave phase velocity, but in this case we have studied for subsonic and supersonic speed of the wave phase (Zel'dovich and Raizer, 1966; Landau and Sykes, 1959).

If we now ignore the viscous effect (i.e., $\eta_0 = 0$), the KdV–Burger equation [Eq. (21)] reduces to the standard KdV equation

https://doi.org/10.1017/S0263034619000764 Published online by Cambridge University Press

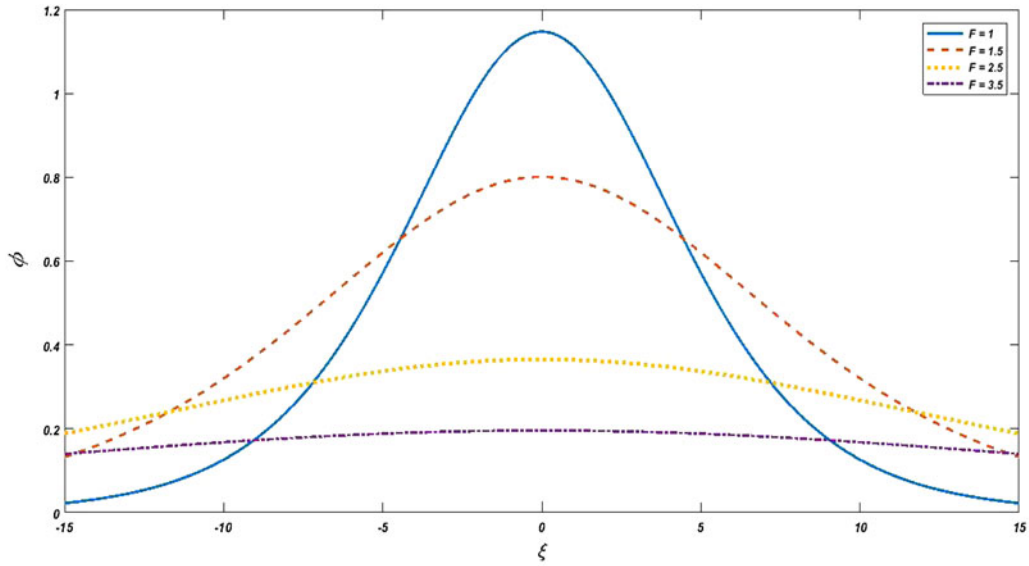

Fig. 19. Solitary structures for different finite temperature electron degeneracy parameter (F) with $M = 0.7$, $u_0 = 0.5$, $\sigma = 0.5$, $H = 2$, and $\chi = 0.5$.

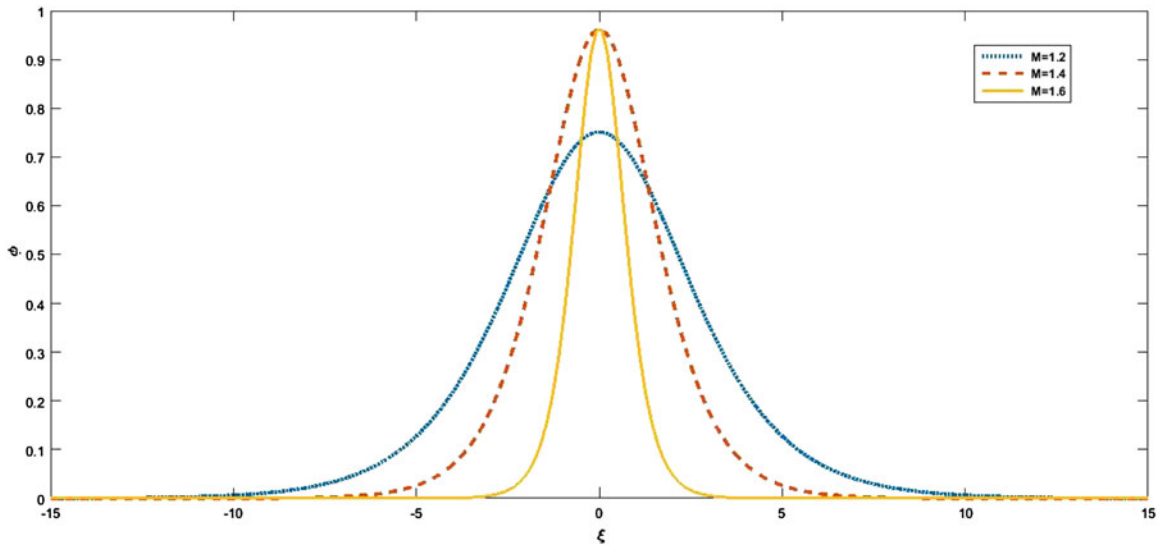

Fig. 20. Solitary structures for different Mach number (M) with $F = 1.5$, $u_0 = 0.5$, $\sigma = 0.5$, $H = 2$, and $\chi = 0.5$.

showing the solitary wave formation. We now study the parametric dependence of the KdV solitary structures. We see that quantum diffraction (H) cannot alter the solitary profile amplitude but can shrink the width (Fig. 18); the electron degeneracy parameter (F) increases both height and width of the profile (Fig. 19). Figure 20 shows that above a certain value $M > 1.4$, the amplitude remains constant but the width shrinks. An electron to ion temperature ratio (σ) cannot alter the width but decreases the amplitude (Fig. 21). The streaming speed decreases the amplitude and widens the profile (Fig. 22). There is no effect of the ratio Fermi and thermal velocity squared (χ) on the solitary profile.

The conclusions that we can now draw from these figures that H is a function of density which shows serious dispersive effects along with nonlinearity, but the effective potential is invariant once the density crosses certain limit (i.e., in quantum range).

Thermal degeneracy effect (shown by F) is rather an important parameter where the statistical effect interferences are strong so as to mitigate quantum tunneling effects. The streaming speed if stays below the critical value of $M_c = 1.4$ can have certain effect in the nonlinear behavior, but once above it, the correlation effects come into play due to the extreme dynamic compactness that the potential remains peaked at the same value, much like the effect of H. Depending upon the thermal inhomogeneity of electrons and ions and the nonequilibrium exchange of energy, the parameter σ can decrease the peak potential slightly but the width remains invariant, implying no dispersion losses.

https://doi.org/10.1017/S0263034619000764 Published online by Cambridge University Press

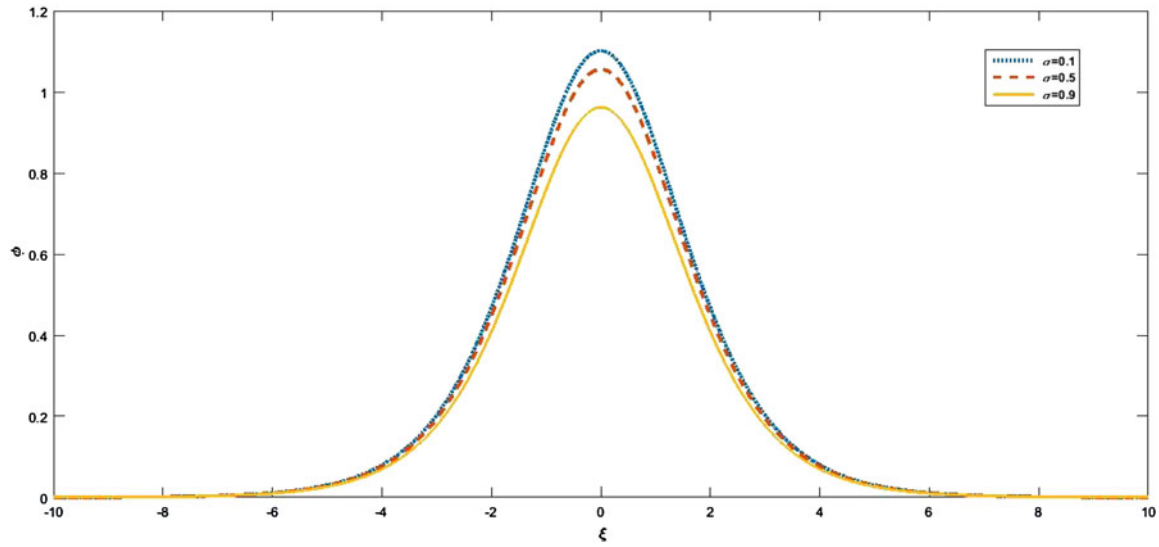

Fig. 21. Solitary structures for different electron to ion temperature ratio (σ) with $F = 1.5$, $u_0 = 0.5$, $\chi = 0.5$, $H = 2$, and $M = 0.7$.

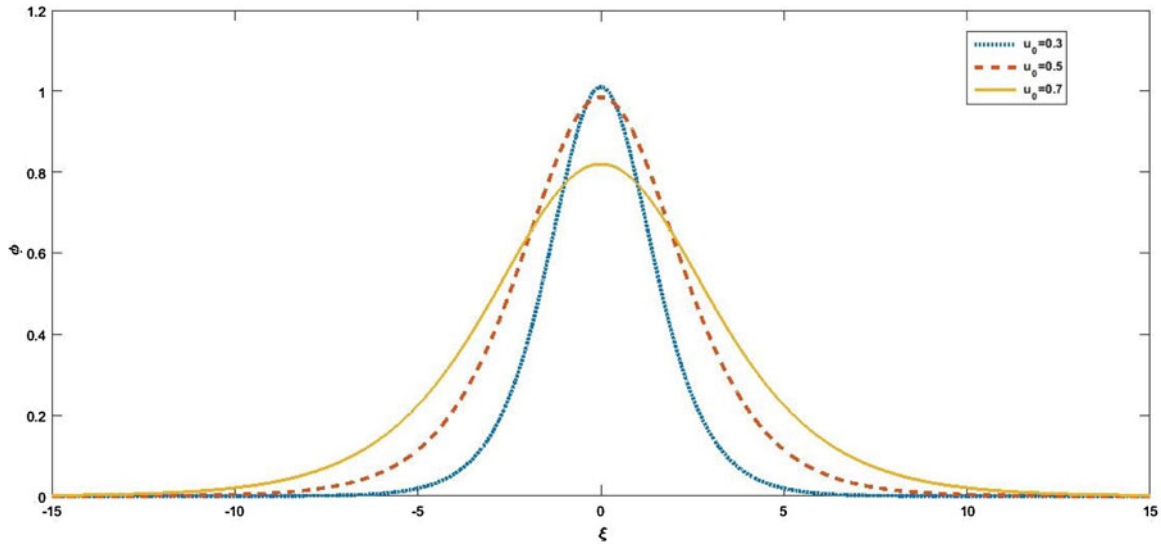

Fig. 22. Solitary structures for different streaming velocity (u_0) with $F = 1.5$, $\sigma = 0.5$, $\chi = 0.5$, $H = 2$, and $M = 0.7$.

Conclusion

To sum up, we have investigated the parametric dependence of linear dispersion characteristics and nonlinear shocks and solitary profiles on various plasma parameters. The effects and the absence of some have been discussed with explanation why they are influential or not in certain ranges. We also found which parameter should be taken care of, if we need to obtain a solitary profile to form an electrostatic shock.

The result obtained here will be helpful in understanding the many laser plasma interaction and space phenomenon experimental situations and help design our equipments to take into considerations of the many situations that the laser-produced plasma thus might undergo. In our coming work, we also plan to incorporate electronic exchange interaction and discussed about the influences.

Acknowledgments. We would like to thank Prof. A. Roy Chowdhury for his inspiration and support. The authors would like to thank Physics Departments of Jadavpur University and Government General Degree College at Kushmandi for providing facilities to carry this work.

References

Akbari-Moghanjoughi M (2012) Shukla-Eliasson attractive force: revisited. *Journal of Plasma Physics* **79**, 189–196.

Akbari-Moghanjoughi M and Eliasson B (2016) Hydrodynamic theory of partially degenerate electron–hole fluids in semiconductors. *Physica Scripta* **91**, 105601.

Bailung H, Sharma S, Bhagoboty N and Nakamura Y (2011) Shock wave propagation in a dusty plasma crystal. *AIP Conference Proceedings* **1397**, 287–288.

https://doi.org/10.1017/S0263034619000764 Published online by Cambridge University Press

Chandra S (2016) Propagation of electrostatic solitary wave structures in dense astrophysical plasma: effects of relativistic drifts and relativistic degeneracy pressure. *Advances in Astrophysics* **1**, 187–200.

Chandra S and Ghosh B (2012) Modulational instability of electron-acoustic waves in relativistically degenerate quantum plasma. *Astrophysics and Space Science* **342**, 417–424.

Chandra S and Ghosh B (2013) Non-linear propagation of electrostatic waves in relativistic fermi plasma with arbitrary temperature. *Indian Journal of Pure and Applied Physics* **51**, 627.

Chandra S, Paul SN and Ghosh B (2012) Linear and non-linear propagation of electron plasma waves in quantum plasma. *Indian Journal of Pure and Applied Physics* **50**, 314–319.

Chandra S, Paul SN and Ghosh B (2013) Electron-acoustic solitary waves in a relativistically degenerate quantum plasma with two-temperature electrons. *Astrophysics and Space Science* **343**, 213–219.

Devanandhan S, Singh SV, Lakhina GS and Bharuthram R (2011) Electron acoustic solitons in the presence of an electron beam and superthermal electrons. *Nonlinear Processes in Geophysics* **18**, 627–634.

Eliezer S, Nissim N, Raicher E and Martínez-Val JM (2014) Relativistic shock waves induced by ultra-high laser pressure. *Laser and Particle Beams* **32**, 243–251.

El-Taibany WF, El-Siragy NM, Behery EE, El-Bendary AA and Taha RM (2019) Dust acoustic waves in a dusty plasma containing hybrid Cairns–Tsallis-distributed electrons and variable size dust grains. *Chinese Journal of Physics* **58**, 151–158.

Esirkepov T, Borghesi M, Bulanov S, Mourou G and Tajima T (2004) Highly efficient relativistic-ion generation in the laser-piston regime. *Physical Review Letters* **92**, 175003.

Ghosh B and Chandra S (2013) Nonlinear surface waves on a quantum plasma half-space with arbitrary temperature. *International Journal of Systems Algorithms and Applications* **3**, 1.

Goswami J, Chandra S and Ghosh B (2019) Shock waves and the formation of solitary structures in electron acoustic wave in inner magnetosphere plasma with relativistically degenerate particles. *Astrophysics and Space Science* **364**, 65. doi:10.1007/s10509-019-3555-7.

Haas F (2011) A fluid model for quantum plasmas. In *Quantum Plasmas*. New York, NY: Springer, pp. 65–93. https://link.springer.com/book/10.1007/978-1-4419-8201-8

Haas F, Garcia LG, Goedert J and Manfredi G (2003) Quantum ion-acoustic waves. *Physics of Plasmas* **10**, 3858–3866. arXiv: https://doi.org/10.1063/1.1609446.

Henis Z, Eliezer S and Raicher E (2019) Collisional shock waves induced by laser radiation pressure. *Laser and Particle Beams* **37**, 268–275.

Hora H (2012) Fundamental difference between picosecond and nanosecond laser interaction with plasmas: ultrahigh plasma block acceleration links with electron collective ion acceleration of ultra-thin foils. *Laser and Particle Beams* **30**, 325–328.

Jagadeesh G (2008) Fascinating world of shock waves. *Resonance* **13**, 752–767.

Lakhina G (1995) Excitation of plasma sheet instabilities by ionospheric O^+ ions. *Geophysical Research Letters* **22**, 3453–3456.

Landau LD and Lifshitz EM (1959) *Fluid Mechanics*. Translated from Russian by J. B. Sykes and W. H. Reid. Oxford, New York, Toronto, Sydney, Paris, Braunschweig: Pergamon Press (reprinted 1975).

Macchi A, Borghesi M and Passoni M (2013) Ion acceleration by superintense laser-plasma interaction. *Reviews of Modern Physics* **85**, 751–793.

Misra A and Bhowmik C (2007) Nonplanar ion-acoustic waves in a quantum plasma. *Physics Letters A* **369**, 90–97.

Naumova N, Schlegel T, Tikhonchuk V, Labaune C, Sokolov I and Mourou G (2009) Hole boring in a dt pellet and fast-ion ignition with ultraintense laser pulses. *Physical Review Letters* **102**, 025002.

Robinson APL, Gibbon P, Zepf M, Kar S, Evans RG and Bellei C (2009) Relativistically correct hole-boring and ion acceleration by circularly polarized laser pulses. *Plasma Physics and Controlled Fusion* **51**, 024004.

Saitou Y, Nakamura Y, Kamimura T and Ishihara O (2012) Bow shock formation in a complex plasma. *Physical Review Letters* **108**, 065004.

Schlegel T, Naumova N, Tikhonchuk V, Labaune C, Sokolov I and Mourou G (2009) Relativistic laser piston model: ponderomotive ion acceleration in dense plasmas using ultraintense laser pulses. *Physics of Plasmas* **16**, 083103.

Schmidt P and Boine-Frankenheim O (2016) A gas-dynamical approach to radiation pressure acceleration. *Physics of Plasmas* **23**, 063106. https://doi.org/10.1063/1.4952623

Shukla PK and Eliasson B (2010) Nonlinear aspects of quantum plasma physics. *Physics-Uspekhi* **53**, 51–76.

Theobald W, Akli K, Clarke R, Delettrez JA, Freeman RR, Glenzer S, Green J, Gregori G, Heathcote R, Izumi N, King JA, Koch JA, Kuba J, Lancaster K, MacKinnon AJ, Key M, Mileham C, Myatt J, Neely D, Norreys PA, Park HS, Pasley J, Patel P, Regan SP, Sawada H, Shepherd R, Snavely R, Stephens RB, Stoeckl C, Storm M, Zhang B and Sangster TC (2006) Hot surface ionic line emission and cold K-inner shell emission from petawatt-laser-irradiated Cu foil targets. *Physics of Plasmas* **13**, 043102.

Wazwaz AM (2008) The tanh method for travelling wave solutions to the Zhiber–Shabat equation and other related equations. *Communications in Nonlinear Science and Numerical Simulation* **13**, 584–592.

Zel'dovich Ya and Raizer Yu (1966) *Physics of Shock Waves and High-Temperature Hydrodynamic Phenomena*, Vol. **1**. Mineola, New York: Dover Publication, pp. 45–68.

https://doi.org/10.1017/S0263034619000764 Published online by Cambridge University Press